METHODS AND APPLICATIONS OF ANALYSIS.
Vol. 17, No. 3, pp. 263–278, September 2010

002

THE PRESSURE GRADIENT SYSTEM*

YUXI ZHENG† AND ZACHARY ROBINSON‡

Abstract. The pressure gradient system is a sub-system of the compressible Euler system. It can be obtained either through a flux splitting or an asymptotic expansion. In both derivations, the velocity field is treated as a small remnant of the original velocity of the Euler system. As such, the boundary conditions for the velocity do not necessarily follow the original ones and careful consideration is needed for the validity, integrity, and completeness of the model. We provide numerical simulations as well as basic characteristic analysis and physical considerations for the Riemann problems of the model to find out appropriate internal conditions at the origin. The study reveals subtle structures of the velocity: Both components exhibit discontinuities at the origin at traditional levels of numerical resolutions around 400×400 cells on the unit square, but they vanish at the origin with possible square root type singularity when we increase the resolutions. Comparing to the roll-up of shear waves or vortex-sheets of the Euler system, these singularities are mild and occur only along rays from the origin. The numerics is done at higher resolutions than traditionally possible via the automated clawpack that contains adaptive mesh refinement (AMR) and message passing interface (MPI), for which we provide the Riemann solvers in both the normal and transversal directions, where the Roe's approximation has the elegant 1/2 average in the model's original variables.

Key words. Dimension splitting, Riemann problem, Roe approximation.

AMS subject classifications. Primary: 35L65, 35J70, 35R35; Secondary: 35J65.

1. Introduction.

The Euler system for compressible ideal gases is an elegant system that reflect the simple physical laws of conservation of mass, momentum, and energy. In one space dimension, the initial value problem has been shown to be well-posed, albeit for data with small total variations. In higher space dimensions, the initial value problem and the simpler Riemann problems are open. Physical experiments and numerical simulations have been done since more than a century ago on various kinds of situations, including the well-known oblique shock reflection on a wedge [6, 11, 8, 9]. Many types of structures are revealed which indicate that higher dimensional problems are very complicated, and simplified models are appreciated. One way to build a model is via the observation that there are two causes for the motion of an ideal gas: One is inertia; i.e., a gas particle is moving because it has been moving, while the other is the gradient of pressure; i.e., a gas particle moves because there is a pressure inequality. Ignoring the simultaneity of the two motions, we can study the two motions individually as simplified models. The pressure gradient system is obtained this way that catches the motion caused by the pressure gradient. Miraculously, the same system can be obtained by considering the Euler system in the limit as the adiabatic gas constant approaches infinity, which is a nonphysical process, but it links the model with the Euler system quantitatively, see Sect. 2.

The pressure gradient system has been studied theoretically since 1995. The main attention has been on its pressure equation which decouples from the velocity. From our experience, however, it seems clear that the velocity affects the pressure field through subtle boundary coupling, including conditions at the origin and shock waves as free boundaries. We set out in this paper to investigate in detail the link between the velocity field and the pressure variable. We find through numerical simulations

*Received February 26, 2010; accepted for publication October 4, 2010.
†Department of Mathematics, The Pennsylvania State University, University Park, PA 16802, USA (yzheng@math.psu.edu).
‡The Pennsylvania State University, University Park, PA 16802, USA (ztr5005@psu.edu).

that the velocity field plays a major role in shock formation, albeit no formation of roll-up of slip lines. Indeed, the velocity must be reduced to zero at the origin — the numerics shows, which is a condition that has not been emphasized.

Our numerical procedure is based on the platform of clawpack, which offers a framework for which we only need to provide the Riemann solvers in the one-dimensional normal direction and a transversal direction. The Riemann solvers are based on Roe average, which has the elegant middle point property for the pressure gradient system (see Sect. 4). The clawpack-compatible code of the Riemann solvers are available on our web site at http://www.math.psu.edu/yzheng/pge. The interested user will find that it is as user friendly as the clawpack. The clawpack is available free-of-charge on its web site.

We point out that there are quite a few numerical simulations on the solutions to Riemann problems for the Euler system, see [17, 14, 20, 13, 10], the earlier four of which by now have shown their ages due to rapid advances of computer technology and theoretical demand of details. We comment that the scheme of Schule-Rinne et. al. [20], based on Roe's average, is automated in the clawpack, which is easy to use for exploring the Euler system. Our emphasis here is to extend the clawpack to cover the pressure gradient system and utilize the convenience of the package to explore important subtle details of solutions, which are shown in the aforementioned papers of simulations, to facilitate theoretical research.

For other models of the Euler system in two space dimensions, we refer the reader to Brio and Hunter [3] for the unsteady transonic small disturbance equation, Canic, Keyfitz and Kim [4] for a nonlinear wave system, or the book [30].

The organization of this paper is as follows. We give the asymptotic derivation in Sect. 2, propose Riemann problems in Sect. 3, and provide Riemann solvers in Sect. 4. We mention the issue of the velocity field of the system in Sect. 5. We focus on Configuration B of two-dimensional Riemann problems in Sect. 6, where our main numerical simulations are presented. We show a sharp image for Configuration C in Sect. 7. We conclude in the final section with the conclusion that the pressure gradient system is a satisfactory model, close to the Euler system, and in showing so we have provided the numerical procedure for readers to carry out their own simulations conveniently.

2. The system. We consider the two-dimensional compressible Euler system

$$\begin{cases} \rho_t + \nabla \cdot (\rho \mathbf{u}) = 0, \\ (\rho \mathbf{u})_t + \nabla \cdot (\rho \mathbf{u} \otimes \mathbf{u} + pI) = 0, \\ (\rho E)_t + \nabla \cdot (\rho E \mathbf{u} + p\mathbf{u}) = 0, \end{cases} \tag{2.1}$$

where ρ is the density, $\mathbf{u}$ is the velocity vector, p is the pressure, $E = |\mathbf{u}|^2/2 + p\rho^{-1}/(\gamma - 1)$ is the total energy density per unit mass, and $\gamma > 1$ is the gas constant. The so-called **pressure gradient system** takes the form

$$\begin{cases} u_t + p_x = 0, \\ v_t + p_y = 0, \\ E_t + (up)_x + (vp)_y = 0, \end{cases} \tag{2.2}$$

where $E = p + (u^2 + v^2)/2$. Cauchy problems for both systems are open.

The Euler system is known to be difficult. Simplified models are desired. Let us consider the special situation in which γ is extremely large while velocity and pressure are small, but the density remains normal; i.e., consider the limiting case

$$\left\{\begin{array}{lcll} \rho & = & \rho_0 \ + & \epsilon\,\tilde{\rho}, \\ \mathbf{u} & = & & \epsilon\,\tilde{\mathbf{u}}, \\ p & = & & \epsilon\,\tilde{p} \end{array}\right. \tag{2.3}$$

where $\epsilon = \frac{1}{\gamma-1}$ in the limit $\gamma \to +\infty$. We typically set $\rho_0 = 1$ for brevity. The variables $(\tilde{\rho}, \tilde{\mathbf{u}}, \tilde{p})$ are what we wish to study. To leading orders of the equations we obtain the pressure gradient system. More precisely, the equation for ρ becomes

$$(\rho_0)_t + \epsilon(\tilde{\rho}_t + \nabla \cdot (\rho_0 \tilde{\mathbf{u}})) + O(\epsilon^2) = 0$$

whose leading order is $(\rho_0)_t = 0$. We let $\rho_0 = 1$. The momentum equation becomes

$$\epsilon(\tilde{\mathbf{u}}_t + \nabla \cdot (\tilde{p} I)) + O(\epsilon^2) = 0$$

whose leading order equation is $\tilde{\mathbf{u}}_t + \nabla \cdot (\tilde{p} I) = 0$. Similarly, the energy equation at order ϵ^2 is the equation shown in the third equation of the pressure gradient system.

In the asymptotic process we note that the sound speed

$$c = \sqrt{\gamma p/\rho} \sim \sqrt{\tilde{p}}$$

remains at order one ($O(1)$), thus our asymptotic system retains acoustic waves.

The pressure decouples from the velocity field to form the pressure gradient equation

$$\left(\frac{p_{\,t}}{p}\right)_t - \Delta p = 0$$

which is indeed simpler than the Euler system, where we have omitted the tilde on p for brevity. The pressure gradient system is the first two-dimensional system of two or more equations to have the existence established of a global regular reflection on a wedge, see the reference Y. Zheng [29]. Other progresses are [2, 7, 12, 15, 21, 22, 27, 28].

We finish this section with a bit of history. The splitting of the Euler system into the flow by pressure difference and the inertia can be traced back to a paper by Li and Cao ([18]) in 1985 and a paper by Agarwal and Halt ([1]) in 1994 for numerical simulations. As a model for theoretical approaches, the system was studied in P. Zhang, J. Li and T. Zhang ([24]) and Y. Zheng ([27]) in 1997-1998, see the books of Li, Zhang, and Yang ([17]) and Zheng ([30]). The asymptotic derivation of this section was formulated in 2003 when Y. Zheng discussed the issue with John Hunter.

3. Riemann problems. We propose Riemann problems as initial-value problems in which the initial values are independent of the spatial radius $r = \sqrt{x^2 + y^2}$, $(x, y) \in \mathbb{R}^2$. Such types of data allow us to look for the so-called *self-similar* solutions that depend only on the variables $\xi = x/t,\ \eta = y/t$. A natural realization of the Riemann problems is to have four constants instead of an arbitrary function of the polar angle θ, see Wagner [23] and Zhang and Zheng [25, 26]. Typically, however, the four constants are further restricted so as to produce a single wave (shock, rarefaction, or slip line) between any two neighboring quadrants, forming the so-called *four-wave Riemann problems.* For the pressure gradient system, the four-wave Riemann problems are classified into 12 nontrivial configurations (A – L), see [17], on top of three obvious cases. We study Configurations B and C in this paper, see Sections 6 and 7.

4. Riemann solver. We consider the one-dimensional Riemann problem for the pressure gradient system

$$\begin{cases} u_t + p_x &= 0, \\ v_t &= 0, \\ E_t + (up)_x &= 0, \end{cases} \tag{4.4}$$

where $p = E - \frac{1}{2}(u^2+v^2)$. We regard $(u, v, E) =: U$ as the primary variables, while the pressure p and the speed of sound $c = \sqrt{p}$ are derived variables. The one-dimensional data are

$$(u, v, E) = (u_i, v_i, E_i), \qquad (i = 1, 2)$$

corresponding to the half spaces $x > 0$ and $x < 0$, respectively, for all y. The system can be cast in the form

$$U_t + F(U)_x = 0$$

or

$$U_t + A(U)U_x = 0$$

for

$$F(U) = [p, \quad 0, \quad up]^T$$

and the Jacobian matrix of $F(U)$:

$$A(U) = F'(U) = \begin{bmatrix} -u & -v & 1 \\ 0 & 0 & 0 \\ p - u^2 & -uv & u \end{bmatrix}.$$

We find that Roe's approximation ([19, 16])is simple for the pressure gradient system. That is,

PROPOSITION 1 (Roe average). *For any two states U_1 and U_2 with nonnegative energy $E_1 \geq 0, E_2 \geq 0$ and nonnegative pressure $p_1 \geq 0$, $p_2 \geq 0$, we have*

$$F(U_2) - F(U_1) = F'(\overline{U})(U_2 - U_1)$$

where $\overline{U} = (U_1 + U_2)/2$ and $\bar{p} = (p_1 + p_2)/2$, and $p_j = E_j - \frac{1}{2}(u_j^2 + v_j^2), j = 1, 2$.

Proof. Let $\Delta w = w_2 - w_1$ for $w = u, v, E, p$. We look for $(\hat{u}, \hat{v}, \hat{E}, \hat{p})$ that solves

$$\begin{bmatrix} \Delta p \\ 0 \\ u_2\Delta p + p_1\Delta u \end{bmatrix} = \begin{bmatrix} -\hat{u} & -\hat{v} & 1 \\ 0 & 0 & 0 \\ \hat{p} - (\hat{u})^2 & -\hat{u}\hat{v} & \hat{u} \end{bmatrix} \begin{bmatrix} \Delta u \\ \Delta v \\ \Delta p + \bar{u}\Delta u + \bar{v}\Delta v \end{bmatrix}. \tag{4.5}$$

From the first row, we find

$$\Delta p = -\hat{u}\Delta u - \hat{v}\Delta v + \Delta p + \bar{u}\Delta u + \bar{v}\Delta v.$$

Since Δu and Δv are independent and arbitrary, we must have

$$\hat{u} = \bar{u}, \quad \hat{v} = \bar{v}.$$

From the third row of the matrix equation and using $\hat{u} = \bar{u}, \hat{v} = \bar{v}$, we find

$$u_2 \Delta p + p_1 \Delta u = \hat{p} \Delta u + \hat{u} \Delta p.$$

Using $\hat{u} = \bar{u}$, we obtain

$$\Delta p(u_2 - \hat{u}) + \Delta u(p_1 - \hat{p}) = 0,$$

which is

$$\Delta p \Delta u/2 + \Delta u(p_1 - \hat{p}) = 0.$$

Canceling Δu from the equation we obtain

$$\hat{p} = \bar{p}.$$

The proof is complete. □

We comment that the value p via the function relation $p = E - \frac{1}{2}(u^2 + v^2)$ at $\overline{U}$ is greater than the value $\bar{p} = (p_1 + p_2)/2$. We use the average $\bar{p} = (p_1 + p_2)/2$ rather than the function evaluation of p through the formula $p = E - \frac{1}{2}(u^2 + v^2)$ at $\overline{U}$. Note that the fluxes for this system and the one-dimensional Burgers' are either quadratic or cubic functions of their variables.

PROPOSITION 2 (Riemann solver). *The Roe average $F'(\overline{U})$ has three eigenvalues $\lambda_1 = -\sqrt{\bar{p}}, \lambda_2 = 0, \lambda_3 = \sqrt{\bar{p}}$ with three corresponding right eigenvectors*

$$\mathbf{r}_1 = \begin{bmatrix} 1 \\ 0 \\ \bar{u} - \sqrt{\bar{p}} \end{bmatrix}, \quad \mathbf{r}_2 = \begin{bmatrix} 0 \\ 1 \\ \bar{v} \end{bmatrix}, \quad \mathbf{r}_3 = \begin{bmatrix} 1 \\ 0 \\ \bar{u} + \sqrt{\bar{p}} \end{bmatrix}$$

and splitting formula

$$\Delta U = \Sigma_{\ell=1}^{3} \beta_\ell \mathbf{r}_\ell$$

where

$$\beta_1 = \frac{-\Delta E + \Delta u(\bar{u} + \sqrt{\bar{p}}) + \bar{v}\Delta v}{2\sqrt{\bar{p}}}, \quad \beta_2 = \Delta v, \quad \beta_3 = \Delta u - \beta_1.$$

Proof. It is straightforward computation, which we omit. The proof is complete. □

The solution to the Riemann problem is therefore approximated by

$$U(\xi) = U_1 + \Sigma_{\lambda_\ell < \xi} \beta_\ell \mathbf{r}_\ell$$

where the summation is over all ℓ for which $\lambda_\ell < \xi$.

From here on, a numerical procedure based on Godunov scheme and the Roe approximation for obtaining an approximate solution has been automated in CLAWPACK. Briefly, it develops the expansion formulas for the differences

$$\begin{aligned} \Sigma_{\ell=1}^{3}\mathcal{W}_{i-1/2}^{\ell} &= U_i - U_{i-1} =: \Delta U_{i-1/2} \\ \mathcal{A}^-\Delta U_{i-1/2} + \mathcal{A}^+\Delta U_{i-1/2} &= F(U_i) - F(U_{i-1}) \end{aligned} \tag{4.6}$$

with

$$\mathcal{A}^-\Delta U_{i-1/2} = (\lambda_1)_{i-1/2}\mathcal{W}_{i-1/2}^1, \quad \mathcal{A}^+\Delta U_{i-1/2} = (\lambda_3)_{i-1/2}\mathcal{W}_{i-1/2}^3,$$

and the the first order Godunov scheme has the form

$$U_i^{n+1} = U_i^n - \frac{\Delta t}{\Delta x}\left[\mathcal{A}^+\Delta U_{i-1/2} + \mathcal{A}^-\Delta U_{i+1/2}\right].$$

For higher-order schemes, the iteration formulas are

$$U_i^{n+1} = U_i^n - \frac{\Delta t}{\Delta x}\left[\mathcal{A}^+\Delta U_{i-1/2} + \mathcal{A}^-\Delta U_{i+1/2}\right] - \frac{\Delta t}{\Delta x}(\tilde{F}_{i+1/2} - \tilde{F}_{i-1/2})$$

where $\tilde{F}_{i-1/2}$ is a limited flux depending on the signs of the eigenvalues.

In two space dimensions, we provide the Riemann solver subroutine rpn2pge.f and the transversal part rpt2pge.f. The normal part rpn2pge is simply the one-dimensional version, but incorporates both the x-direction and the y-directions. The transversal part is a two-dimensional phenomena, which does not appear in one space dimension.

The dimensional splittings, including Strang splitting, adaptive mesh refinements, and message passing interface are automated in CLAWPACK for direct applications on the pressure gradient system.

5. The issue of velocity. There is concern about how to impose boundary conditions on the velocity (u, v) for the pressure gradient system, both physical boundary conditions and internal boundary conditions and particularly the values of (u, v) at the spatial origin. Take, for examples, the Riemann data with two lines of symmetry, such as Configurations B and C, see below, it is an issue as to how to impose velocity conditions at the origin. Once a decoupled pressure p is solved from the second-order equation for p, one can integrate the momentum equations to find (u, v) all the way to the origin, which seem to give possibly nonvanishing values of (u, v) at the origin. For the Euler system, there is no question as to requiring the velocity to vanish at the origin. However, the velocity for the pressure gradient system is a high-order term of the Euler system and it is not clear whether we should impose similar conditions on it. The boundary behavior of the velocity is one of the main points of this paper. We use numerics to show that velocity at the origin for the pressure gradient system does vanish – albeit very slowly – for Configurations B and C. For the Euler system, numerics indicates that the velocity also vanishes and it manages to do so by allowing the density function to develop local extrema near the origin.

6. Configuration B. In Configuration B, the four states $\{(p_i, u_i, v_i)\}$ for i-th quadrants $(i = 1, 2, 3, 4)$ are such that a single rarefaction wave of the plus family is produced between states 1 and 2 across the positive y-axis, a single rarefaction wave of the minus family is produced between states 2 and 3 across the negative x-axis, a single rarefaction wave of the plus family is produced between states 3 and 4 across the negative y-axis, and a single rarefaction wave of the minus family is produced

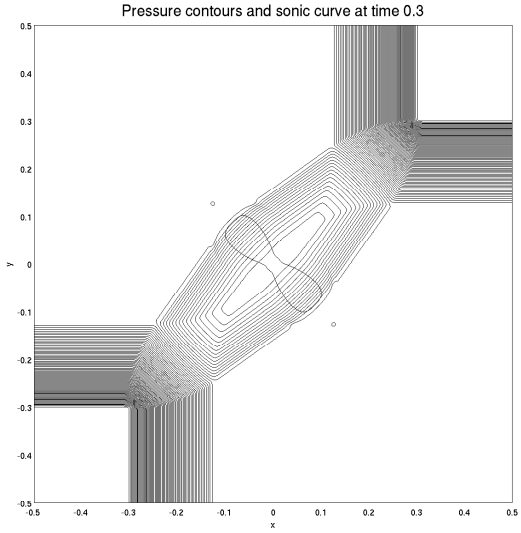

FIG. 1. *Contour lines of pressure at* $c_2 = 0.42, c_1 = 1.0$. *For theoretical interests, we have plotted the pseudo-Mach number contour at 1.0, which is the double-lobe closed curve.*

between states 4 and 1, see p.193 of [17]. This is the case which we also call *bi-symmetric four rarefaction wave interaction*. The only free parameter in this case is the pressure in quadrant two: $p_2 \in [0, 1]$, since we normalize the state in quadrant one so that $p_1 = 1$ and require the lines of symmetry to pass through the origin. We choose data $c_2 (= \sqrt{p_2})$ from $(0, 1]$ and use the data

$$\begin{array}{lll} p_1 = 1, & u_1 = 1 - c_2, & v_1 = u_1; \\ p_2 = c_2^2, & u_2 = -u_1, & v_2 = u_1; \\ p_3 = p_1, & u_3 = -u_1, & v_3 = -u_1; \\ p_4 = p_2, & u_4 = u_1, & v_4 = -u_1. \end{array} \tag{6.7}$$

In the clawpack, there are a data file to enter c_2, another file to specify the Riemann data (6.7), and a third data file to specify the domain size, final time of computation, number of cells to use and various levels of scheme parameters such as orders of accuracy, etc. We typically choose the computational box to be $[-0.5, 0.5] \times [-0.5, 0.5]$ and final time t up to 0.3. Number of cells along either the coordinate axes is 1600 or fewer, and the slope limiter is minmod. Our number of contour lines used in the matlab display ranges from 60 to 360, depending on the purposes of illustrations. No artificial removal of contours is performed.

We have experimented with various values of c_2. For any c_2 greater than 0.42, the numerical results are quite similar. For c_2 below 0.42, the scheme does not seem to work well, which may be because the solutions are quite close to vacuum, a typical problem for Roe solvers. We use $c_2 = 0.42$ for the presentation in this paper. In Figures 1, 2, and 3, we show the contour plots of the pressure, velocity components u and v, respectively.

We find seemingly that there are slip lines (discontinuous shear waves) at the origin. One slip line is in the horizontal direction in the component of u, while the other is in the vertical direction in the component of v, see Figures 4 - 6. The slip

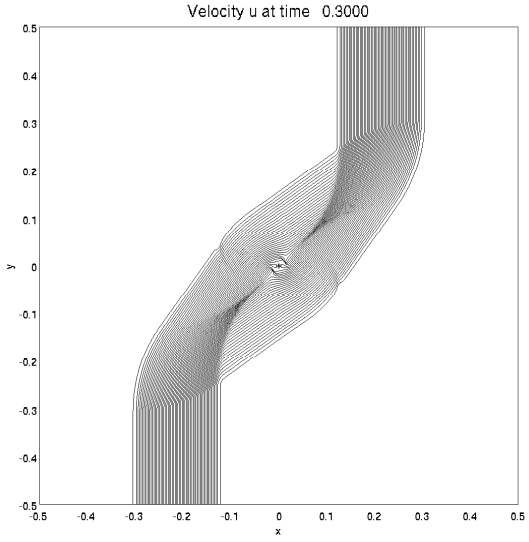

FIG. 2. *Contour lines of u-component of velocity at* $c_2 = 0.42, c_1 = 1.0$.

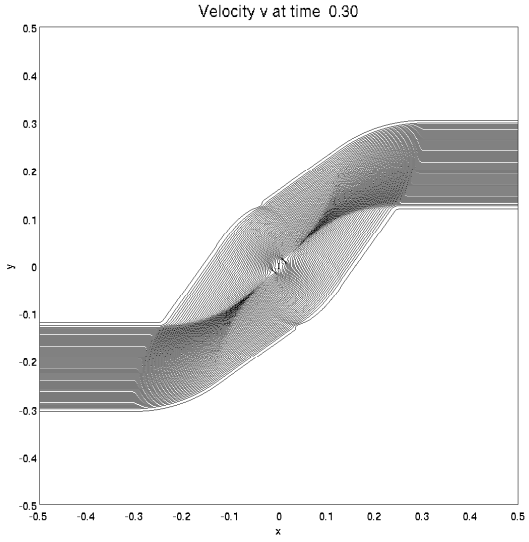

FIG. 3. *Contour lines of v-component of velocity at* $c_2 = 0.42, c_1 = 1.0$.

lines are compatible with the pressure gradient system since the two equations

$$-\xi u_\xi - \eta u_\eta + p_\xi = 0, \quad -\xi v_\xi - \eta v_\eta + p_\eta = 0$$

are both satisfied at the origin as $\nabla p = 0$ at the origin. However, if p is not a constant in the region, then it is unclear how the slip lines satisfy the equations.

For comparison, we show that the density in Figure 7 for the Euler with $c_2 = 0.5$

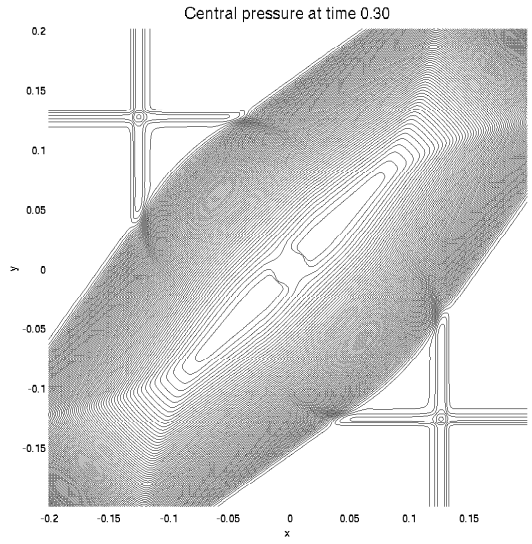

FIG. 4. *Central contour lines of pressure at* $c_2 = 0.42, c_1 = 1.0$. *More contours are used than Figure 1 for details. The two crosses are numerical errors.*

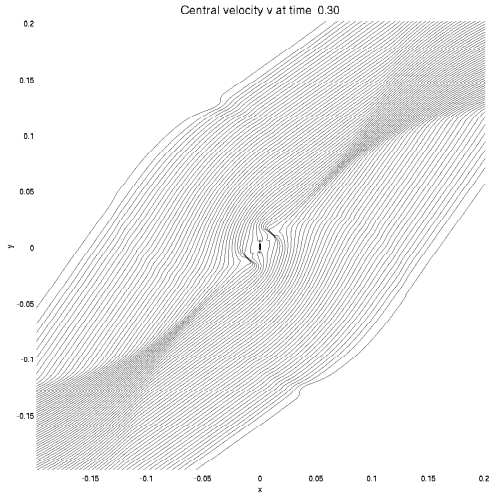

FIG. 5. *Central contour lines of* v *at* $c_2 = 0.42, c_1 = 1.0$.

and the corresponding velocity u in Figure 8. We observe that u is continuous at the origin.

In Figure 9 (a chart), we illustrate the strength of the slip line in v as we refine the grid points. In Figure 10 (an illustration), we explain how we take the measurements for Figure 9.

From the convergence study in Figure 9, we believe that the slip strength tends to zero eventually. To support that idea, we plot the (negative) velocity v against the

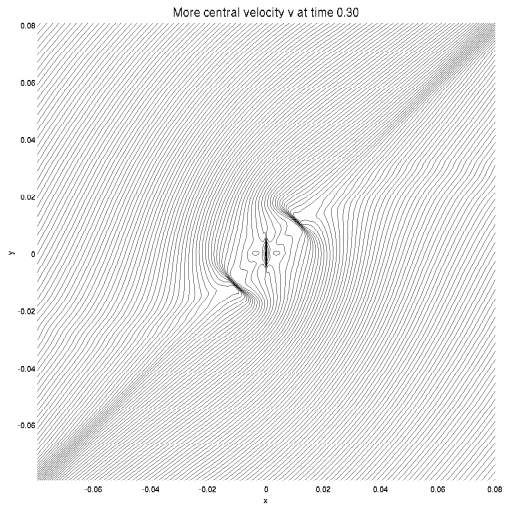

FIG. 6. *Core portion of contour lines of v at $c_2 = 0.42, c_1 = 1.0$.*

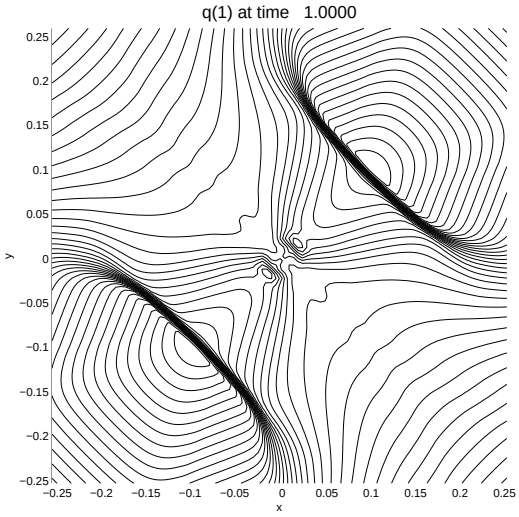

FIG. 7. *Core portion of contour lines of density of Euler at $c_2 = 0.5, c_1 = 1.0$.*

positive x axis (at $y = 0$) in Figure 11, where we also include the best fit of the data in the form of a power function. The best fit power function is

$$v = 0.95x^{0.48}$$

whose derivative blows up at the origin.

Upon close examination we find that the distances in Figure 9 are comparable to individual numerical cell sizes. Thus, we by-pass the plot tools of Matlab and read the numerical data directly to plot v vs. x along the line $y = 0$ in Figures 12,13,14

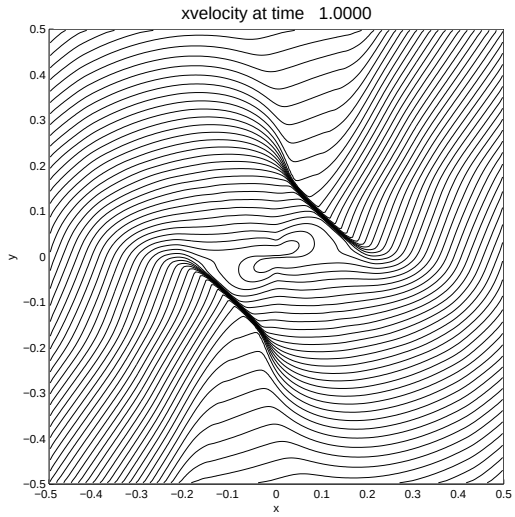

FIG. 8. *Core portion of contours of u-component of Euler at* $c_2 = 0.5, c_1 = 1.0$.

Table: Strength of slip in v with regards to refinement of grids for PGE.

	200x200 cells	400x400 cells	800x800 cells	1600x1600 cells
Δv (at y=0)	0.106904	0.079604	0.060277	0.042552
Δx	0.005400	0.003000	0.001400	0.000880
Δv / Δx	19.80	26.53	43.06	48.36
Δv (at y=L)	0.068724	0.039802	0.026371	0.016066
y length: 2L	0.0250	0.0220	0.0150	0.0106

FIG. 9. *Strength of shear in v-component of velocity of the pressure gradient system at* $c_2 = 0.42, c_1 = 1.0$.

for cell numbers $400^2, 800^2$, and 1600^2, at various zoom levels. Ignoring the peaks of v at the origin, we see a trend of v that tends to be a C^1 smooth function.

In conclusion, we believe that the velocity is at least a continuous function at the origin, it is at worst a power function of the radius with a positive power less than one.

7. Configuration C. In Configuration C, the four states $\{(p_i, u_i, v_i)\}$ for i-th quadrants $(i = 1, 2, 3, 4)$ are such that a single shock of the minus family is produced between states 1 and 2 across the positive y-axis, a single shock of the plus family is produced between states 2 and 3 across the negative x-axis, a single shock of the minus family is produced between states 3 and 4 across the negative y-axis, and a

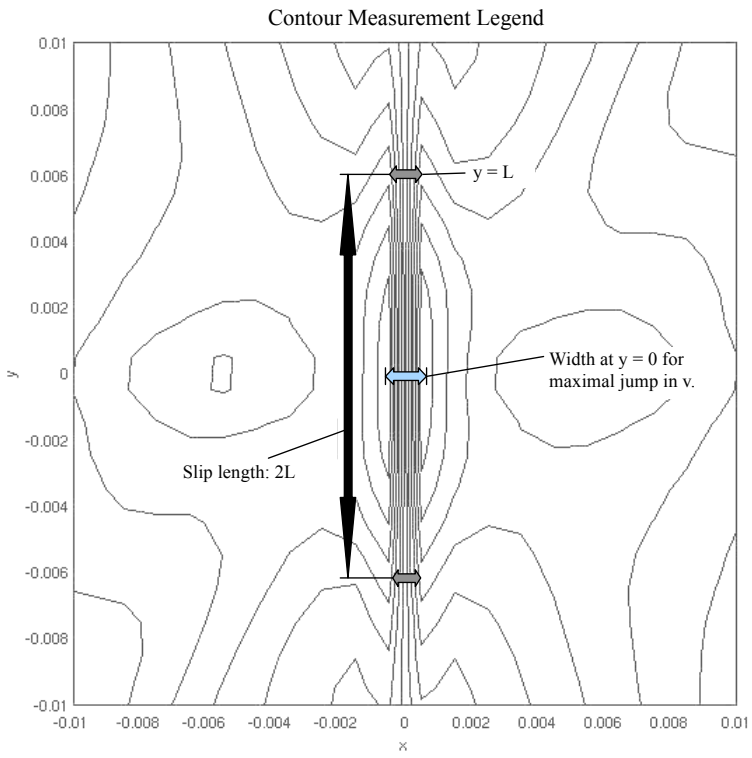

FIG. 10. *Notation in measurement of slip properties.*

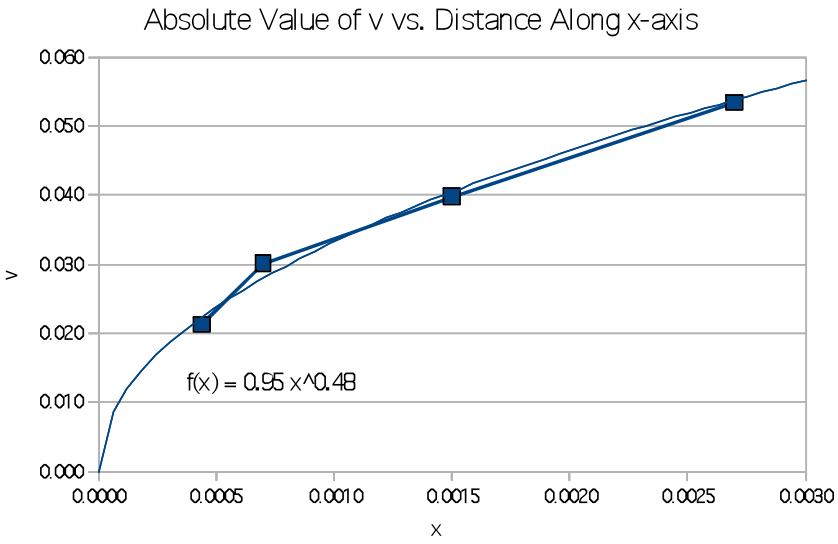

FIG. 11. *Power function fit of the velocity v along the positive x axis for numerical simulations with cells $200^2, 400^2, 800^2$ and 1600^2. The values of v and x are half of the data $\Delta v, \Delta x$ from Figure 9.*

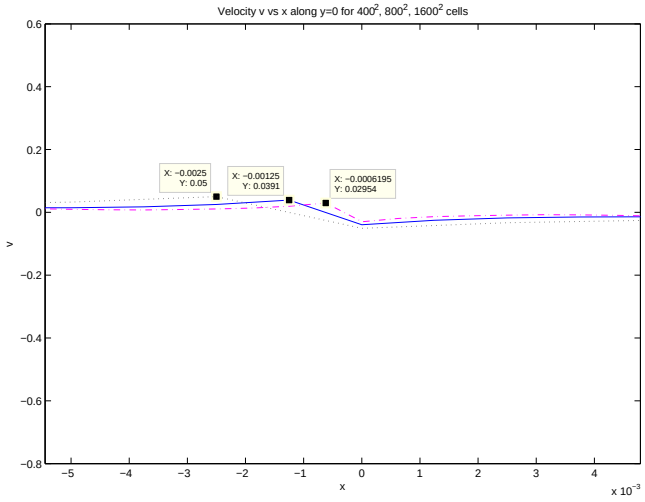

FIG. 12. *Core portion of velocity v along the x axis for numerical simulations with cells* 400^2 *(dotted curve),* 800^2 *(solid curve), and* 1600^2*. (Horizontally zoomed in.)*

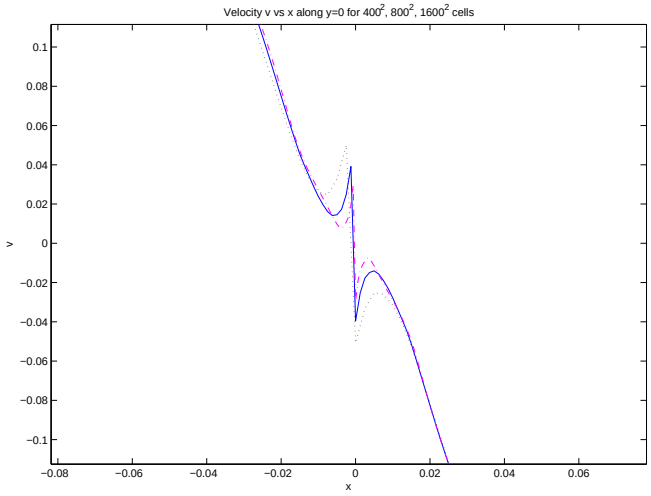

FIG. 13. *Central portion of velocity v along the x axis for numerical simulations with cells* 400^2 *(dotted curve),* 800^2 *(solid curve), and* 1600^2*. (Zoomed in equally in x and y.*

single shock of the plus family is produced between states 4 and 1, see p.195 of [17]. This is the case which we also call *bi-symmetric four shock wave interaction.* The only free parameter is the pressure in quadrant two: $p_2 \in [0, 1]$, since we normalize the state in quadrant one so that $p_1 = 1$ and require the lines of symmetry to pass

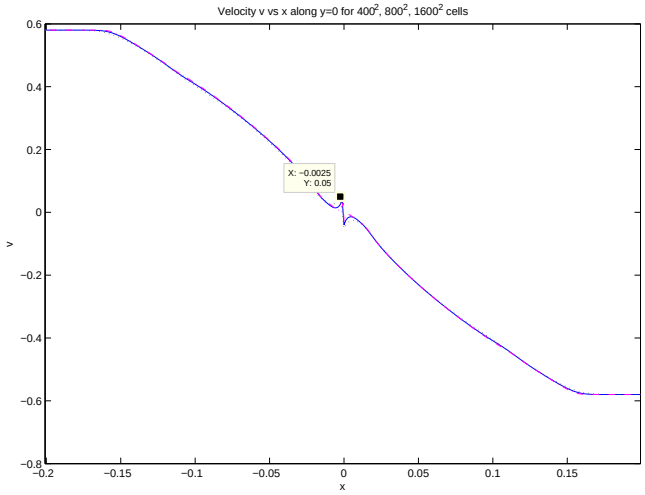

FIG. 14. *Velocity v along the x axis for numerical simulations with cells* 400^2 *(dotted curve),* 800^2 *(solid curve), and* 1600^2.

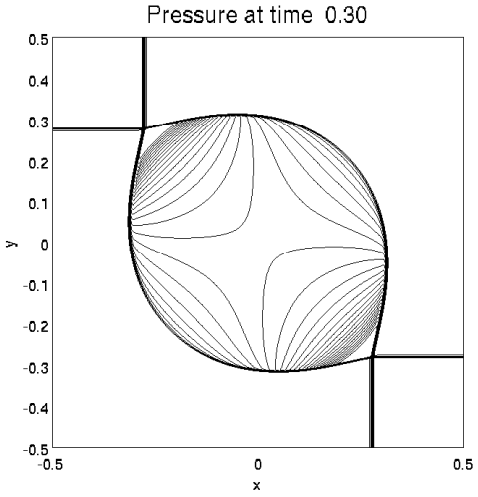

FIG. 15. *Contour lines of pressure for Configuration C at* $c_2 = 0.85, c_1 = 1.0$.

through the origin. We choose data $c_2 = \sqrt{p_2}$ from $(0, 1]$ and use the data

$$
\begin{array}{lll}
p_1 = 1, & u_1 = -(1 - c_2^2)/\sqrt{2(1 + c_2^2)}, & v_1 = u_1; \\
p_2 = c_2^2, & u_2 = -u_1, & v_2 = u_1; \\
p_3 = p_1, & u_3 = -u_1, & v_3 = -u_1; \\
p_4 = p_2, & u_4 = u_1, & v_4 = -u_1.
\end{array} \tag{7.8}
$$

We typically choose the computational box to be $[-0.5, 0.5] \times [-0.5, 0.5]$ and time t up to 0.3.

We note from [24] and [17] that there are subcases in Configuration C. One is for $p_2/p_1 \in (\frac{2}{3}, 1)$ when the state 5 produced by the shocks S_{12}^- and S_{23}^+ is hyperbolic;

one is for $p_2/p_1 \in (4\sqrt{2}-5, \frac{2}{3})$ when the state 5 produced by the shocks S_{12}^- and S_{23}^+ is elliptic, and the third is for $p_2/p_1 < 4\sqrt{2}-5$ when state 5 does not exist. We show in Figure 15 the pressure contour lines for the choice of $c_2 = 0.85$ so that $p_2 = c_2^2 = 0.85^2 \in (2/3, 1)$. The velocity field here seems to be smoother than in Configuration B, thus we believe that the velocity field is continuous at the origin.

8. Conclusion. We introduce with details the model pressure gradient system. The behavior of velocity at the origin is addressed. We provide Roe type Riemann solvers rpn2pge.f and rpt2pge.f in numerics to show that the velocity field of the system vanishes at the origin. The numerics indicate that the pressure gradient system behaves well in its velocity field with a profile no worse than $v = 0.95x^{0.48}$. Its closeness to the Euler system is satisfactory.

We use clawpack, see `http://www.amath.washington.edu/~claw/`. With clawpack, one can do experiments on other Configurations A and D–L. The Riemann solvers rpn2pge.f and rpt2pge.f are available on our web page `http://www.math.psu.edu/yzheng/pge`.

Acknowledgment. The authors would like to thank Jiequan Li and Kyungwoo Song for helpful suggestions. This work is partially supported by NSF DMS-0603859.

REFERENCES

[1] R. K. Agarwal and D. W. Halt, *A modified CUSP scheme in wave/particle split form for unstructured grid Euler flow*, in "Frontiers of Computational Fluid Dynamics", D. A. Caughey and M. M. Hafez, eds., 1994.

[2] S. Bang, *Interaction of three and four rarefaction waves of the pressure-gradient system*, J. Diff. Equations, 246 (2009), pp. 453–481.

[3] M. Brio and J. K. Hunter, *Irregular reflection of weak shocks*, Hyperbolic problems: theory, numerics, applications (Stony Brook, NY, 1994), pp. 347–353, World Sci. Publ., River Edge, NJ, 1996.

[4] S. Canic, B. Keyfitz, and E. H. Kimi, *Free boundary problems for nonlinear wave systems: Mach stems for interacting shocks*, SIAM J. Math. Anal., 37 (2006), pp. 1947–1977.

[5] T. Chang, G. Q. Chen, and S. L. Yang, *On the 2–D Riemann problem for the compressible Euler equations, I. Interaction of shock waves and rarefaction waves*, Disc. Cont. Dyna. Syst., 1:4, (1995), pp. 555–584.

[6] R. Courant and K. O. Friedrichs, *Supersonic flow and shock waves*, Interscience Publishers, Inc., New York, 1948.

[7] Z. Dai and T. Zhang, *Existence of a global smooth solution for a degenerate Goursat problem of gas dynamics*, Arch. Ration. Mech. Anal., 155 (2000), pp. 277–298.

[8] H. M. Glaz, P. Colella, I. I. Glass, and R. L. Deschambault, *A numerical study of oblique shock-wave reflections with experimental comparisons*, Proceedings of the Royal Society of London, Series A, 398 (1985), pp. 117-140.

[9] I. I. Glass and J. P. Sislian, *Nonstationary Flows and Shock Waves*, Oxford Science Publications, 1994.

[10] J. Glimm, X. Ji, J. Li, X. Li, P. Zhang, T. Zhang, and Y. Zheng, *Transonic shock formation in a rarefaction Riemann problem for the 2-D compressible Euler equations*, SIAM J. Appl. Math., 69 (2008), pp. 720–742.

[11] J. Glimm and A. Majda, *Multidimensional Hyperbolic Problems and Computations*, IMA Vol. 29, Springer 1991.

[12] E. H. Kim and K. Song, *Classical solutions for the pressure-gradient equation in the non-smooth and nonconvex domain*, J. Math. Anal. Appl., 293 (2004), pp. 541—550.

[13] A. Kurganov and E. Tadmor, *Solution of two-dimensional Riemann problems for gas dynamics without Riemann problem solvers*, Numer. Methods Partial Differential Equations, 18 (2002), pp. 584–608.

[14] P. Lax and X. Liu, *Solutions of two–dimensional Riemann problem of gas dynamics by positive schemes*, SIAM J. Sci. Compt., 19:2 (1998), pp. 319–340.

[15] Z. Lei and Y. Zheng, *A complete global solution to the pressure gradient equation*, J. Differential Equations, 236 (2007), pp. 280–292.

[16] R. J. LeVeque, *Finite Volume Methods for Hyperbolic Problems*, Cambridge University Press, 2002

[17] J. Li, T. Zhang, and S. Yang, *The two-dimensional Riemann problem in gas dynamics*, Pitman monographs and surveys in pure and applied mathematics 98, Addison Wesley Longman limited, 1998.

[18] Y. Li and Y. Cao, *Second order "large particle" difference method*, Science in China (in Chinese), series A, 8 (1985), pp. 1024–1035.

[19] P. L. Roe, *Approximate Riemann solvers, parameter vectors, and difference schemes*, J. Comput. Phys., 43 (1981), pp. 357–372.

[20] C. W. Schulz–Rinne, J. P. Collins and H. M. Glaz, *Numerical solution of the Riemann problem for two–dimensional gas dynamics*, SIAM J. Sci. Compt., 4 (1993), pp. 1394–1414.

[21] K. Song, *The pressure-gradient system on non-smooth domains*, Comm. Partial Differential Equations, 28 (2003), pp. 199–221.

[22] K. Song and Y. Zheng, *Semi-hyperbolic patches of solutions of the pressure gradient system*, Disc. Cont. Dyna. Syst., series A, 24 (2009), pp. 1365–1380.

[23] D. H. Wagner, *The Riemann problem in two space dimensions for a single conservation law*, SIAM J. Math. Anal., 14 (1983), pp. 534–559.

[24] P. Zhang, J. Li, and T. Zhang, *On two-dimensional Riemann problem for pressure-gradient equations of Euler system*, Discrete and Continuous Dynamical Systems, 4 (1998), pp. 609–634.

[25] T. Zhang and Y. Zheng, *Two-dimensional Riemann problems for a single conservation law*, Trans. AMS, 312 (1989), pp. 589–619.

[26] T. Zhang and Y. Zheng, *Conjecture on the structure of solution of the Riemann problem for two-dimensional gas dynamics systems*, SIAM J. Math. Anal., 21 (1990), pp. 593–630.

[27] Y. Zheng, *Existence of solutions to the transonic pressure-gradient equations of the compressible Euler equations in elliptic regions*, Comm. Partial Differential Equations, 22 (1997), pp. 1849–1868.

[28] Y. Zheng, *A global solution to a two-dimensional Riemann problem involving shocks as free boundaries*, Acta Mathematicae Applicatae Sinica (English series), 19 (2003), pp. 559–572.

[29] Y. Zheng, *Two-dimensional regular shock reflection for the pressure gradient system of conservation laws*, Acta Mathematicae Applicatae Sinica, 22:2 (2006), pp. 177–210 (English series).

[30] Y. Zheng, *Systems of Conservation Laws: Two-Dimensional Riemann Problems*, 38 PNLDE, Birkhäuser, Boston, 2001.